

# Morphology of clusters of attractive dry and wet self-propelled spherical particle suspensions

Francisco Alarcón

*Departament de Física de la Matèria Condensada,  
Universitat de Barcelona, C. Martí Franqués 1, 08028-Barcelona, Spain and  
University of Barcelona Institute of Complex Systems (UBICS), Universitat de Barcelona, Barcelona, Spain.*

Chantal Valeriani

*Departamento de Física Aplicada I, Facultad de Ciencias Física,  
Universidad Complutense de Madrid, 28040 Madrid, Spain.*

Ignacio Pagonabarraga

*Departament de Física de la Matèria Condensada,  
Universitat de Barcelona, C. Martí Franqués 1, 08028-Barcelona, Spain and  
University of Barcelona Institute of Complex Systems (UBICS), Universitat de Barcelona, Barcelona, Spain.*

In order to assess the effect of hydrodynamics in the assembly of active attractive spheres, we simulate a semi-dilute suspension of attractive self-propelled spherical particles in a quasi two dimensional geometry comparing the case with and without hydrodynamics interactions. To start with, independently on the presence of hydrodynamics, we observe that depending on the ratio between attraction and propulsion, particles either coarsen or aggregate forming finite-size clusters. Focusing on the clustering regime, we characterize two different clusters parameters, i.e. their morphology and orientational order, and compare the case when active particles behave either as pushers or pullers (always in the regime where inter-particles attractions competes with self-propulsion). Studying cluster phases for squirmers with respect to those obtained for active Brownian disks (indicated as ABP), we have shown that hydrodynamics alone can sustain a cluster phase of active swimmers (pullers), while ABP form cluster phases due to the competition between attraction and self propulsion. The structural properties of the cluster phases of squirmers and ABP are similar, although squirmers show sensitivity to active stresses. Active Brownian disks resemble weakly pusher squirmer suspensions in terms of cluster size distribution, structure of the radius of gyration on cluster size and degree of cluster polarity.

## I. INTRODUCTION

Active matter is concerned with the study of systems composed of self-driven units and active particles, able of converting energy into systematic movement [1]. Examples of active matter are found from micro to nano length scales, in living or nonliving systems, such as cells, tissues and living organisms, animal groups, self-propelled colloids and artificial nanoswimmers [2–4]. One important feature of active matter is that its elements can develop coordinated behaviour, such as collective motion [5].

Experiments in this field are developing at a rapid pace [6–9] and a new theoretical framework is needed to establish a “universal” behaviour among these internally driven systems. With this goal in mind, a suspension of self-propelled Brownian particles with short-range repulsions, no hydrodynamic interactions (HI) and a spherical shape (thus no steric effects induced by an elongated shape) has been considered as a characteristic, reference system.

Given a suspension of spherical repulsive active Brownian particles (ABP), it has been shown that one can derive an expression for the pressure [10–14], even though the mechanical pressure might not lead to an equation of state [15]. When dealing with dense suspensions, both numerical simulations and theory have identified a motility

induced phase separation [16–22] in (quasi) two (in bulk or under confinement [23]) and three dimensions.

However, when switching on an inter-particle attraction, the phase behaviour of a dilute suspension of attractive spheres is still a matter of debate [24]. Attractive self-propelled spheres aggregate either into a network-forming phase, characterized by a local alignment (without aligning interactions) [25] at high density, or into a (steady state) cluster phase at low densities [26, 27]. The latter has been also observed in a dilute suspension of self-propelled spheres interacting via an isotropic short-range attraction and long-range repulsion [28].

When considering the effect of hydrodynamic interactions, numerical studies of a two dimension suspension of self-propelled repulsive spheres have shown that hydrodynamics suppresses motility induced phase separation in dense suspensions [29], as suggested in the early work by Ishikawa [30], and has an effect in the dynamics of transient clusters at lower densities [31].

Particle’s shape has a strong impact in the collective behavior of suspensions of self-propelled particles. It has been shown that repulsive active rods exhibit a phase-separated state characterized by the formation of polar clusters [32]. Similarly, dilute suspensions of active dumbbells form rotating clusters when particles interact both via a short-range attraction and long-range repul-

sion [28] and an isotropic attraction [33], in the latter case displaying a nematic order with spiral patterns in two dimensions [34].

Inspired by experiments on dilute suspensions of colloids [35] and bacteria [33], showing cluster formation, and motivated by understanding how hydrodynamics could affect the formation of living clusters [27, 28, 36], we have carried out a systematic numerical analysis on dilute 2D suspensions of attractive self-propelled spheres both in the presence (wet active system) and absence (dry active system) of hydrodynamic interactions [37]. We identify the conditions at which the system forms clusters, and characterize their morphology considering and neglecting hydrodynamics. The comparison will provide further insight into the nature of the cluster phases in systems of attractive self-propelled spheres and their main features. Moreover, our study underlines the relevance of active stresses in the collective motion of active suspensions of spheres with attractive interactions.

We perform Lattice-Boltzmann simulations of microswimmers modelled as squirmers [38] (to reproduce the induced hydrodynamic flow around a spherical swimmer while preserving the main features of the active stresses generated by it [39]). Both the character of hydrodynamic active stress, either pushers or pullers,  $\beta$  (entering through its sign) and the magnitude of the swimmer activity affect the qualitative behaviour of a squirmer suspension, as already shown for squirmers close to a solid wall [40] and when studying their rheological properties [41]. Tuning both activity and attraction we are able to characterize different types of collective behaviour, distinguishing pushers from pullers (since depending on the hydrodynamic signature hydrodynamically interacting squirmers can develop long-time polar order [42]) and quantify to what extent an explicit attraction between particles can affect their phase behaviour. To compare with the analogous system without hydrodynamics, we perform Brownian dynamics simulations of a 2D suspension of active Brownian disks (indicated as ABP in the text) [25, 27]. Differently from Ref. [43], on the one hand we take into account hydrodynamics in three dimensions (or quasi 2D); on the other hand, in the absence of hydrodynamics, we consider both translational and rotational diffusion.

The manuscript is organized as follows. In section II we present both the squirmer and the spherical active Brownian disk models. Next, we describe the interaction potential and introduce the parameters and analysis tools used to characterize the different collective behaviour. In section III we present our results, analysing the dynamics of cluster formation and discussing the different clustering regimes depending on the interaction strength versus activity. Finally, we discuss our conclusions in section IV.

## II. SIMULATION DETAILS

### A. Squirmers

We now introduce a hybrid scheme which resolves individual squirmers and the corresponding motion of the embedding fluid in a quasi two dimensional set-up. This approach allows us to consistently follow the dynamics of the fluid and the suspended squirmers on the same footing.

According to the squirmer model (Appendix V A) the solvent velocity,  $\mathbf{u}|_{R_p}$ , on the surface of a spherical squirmer of radius  $R_p$  can be expressed as

$$\mathbf{u}|_{R_p} = [B_1 \sin \theta + B_2 \sin \theta \cos \theta] \boldsymbol{\tau}, \quad (1)$$

where  $\boldsymbol{\tau}$  is a unit vector tangential to the particle surface and the squirmer moves along the direction  $\mathbf{e}_1$  rigidly bound to the particle. identifying an intrinsic axis from which the polar angle  $\theta$  can be determined.

We restrict ourselves to the simplest squirmer model where the slip velocity depends only on two parameters:  $B_1$  that quantifies the asymptotic self-propelling speed,  $v_s = \frac{2}{3}B_1$ , at which an isolated squirmer will swim, and  $B_2$ , proportional to the active stress generated by the squirmer. The ratio between the self-propelling velocity and active stress,  $\beta = B_2/B_1$  [44], quantifies the active state of the squirmers and their interaction with the fluid.  $\beta > 0$  corresponds to pullers, generating a thrust in front of their body, differently from pushers ( $\beta < 0$ ) where the thrust is generated at their back [45]. To simulate squirmers we disregard thermal fluctuations: velocity fluctuations are simply induced by the particles' activity ( $B_2$ ) acting as an effective temperature when competing with conservative forces.

The surrounding fluid is modelled using a Lattice Boltzmann (LB) approach. The solvent is described in terms of the one-particle distribution function,  $f_i(\mathbf{r}, t)$  i.e. the density of a particle with velocity  $\mathbf{c}_i$  at a node ( $\mathbf{r}$ ) of a given lattice. The discretized velocities join nodes and prescribe the lattice connectivity. We use the D3Q19 lattice, characterized by 19 velocities joining nodes of a cubic three dimensional lattice [46]. The fluid dynamics emerge from the evolution of the one-particle distribution function,

$$f_i(\mathbf{r} + \mathbf{c}_i, t + 1) = f_i(\mathbf{r} + \mathbf{c}_i, t) + \Delta_i(\mathbf{r}, t) \quad (2)$$

where  $\Delta_i$  can be understood as the linearised Boltzmann collision operator that relaxes the densities toward a local equilibrium and conserves mass and momentum. This LB model reproduces the dynamics of a Newtonian liquid of shear viscosity  $\eta$  and the relevant hydrodynamic variables are recovered as moments of the one-particle velocity distribution functions [47].

In our simulations particles (with a diameter  $\sigma$  of 4.6 lattice nodes [48]) are individually resolved, imposing a modified bounce back rule for spherical colloids on the one-particle velocity distribution functions for nodes

crossing the solid interface moving from a node outside to one inside the particle (including the slip velocity to impose the squirming motion [40]). The total force and torque the fluid exerts on the particle is obtained by imposing that the total momentum exchange between the solid particle and the fluid nodes vanishes (as a result of the modified bounce back). Accounting for all forces acting on each squirmer allows to update them dynamically. In particular, the torque exerted by the fluid determines how the squirmer direction of selfpropulsion,  $\mathbf{e}_1$  will rotate. In our work we have used a LB code which consists of moving particles via a domain decomposition and parallelization (using MPI) [49] to exploit the excellent scalability of LB on supercomputing facilities.

We simulate attractive squirmers via a truncated and shifted Lennard-Jones potential, of magnitude

$$V(r) = 4\epsilon \left[ \left(\frac{\sigma}{r}\right)^{12} - \left(\frac{\sigma}{r}\right)^6 \right]; \quad (3)$$

when two squirmers are at a distance  $r$  smaller than  $r_{cut} = 2.5\sigma$ , and vanishing otherwise. The competition between attractive and self-propelling forces is quantified through the dimensionless parameter

$$\xi = \frac{F_d}{F_{LJ}}, \quad (4)$$

where  $F_d = 6\pi\eta R_p v_s$  is a characteristic magnitude of the friction force associated to the squirmer self propulsion and  $F_{LJ}$  is the absolute value of the of Lennard-Jones force at its minimum  $r = (26/7)^{1/6}\sigma$ .

We will analyse the dynamics of squirmer suspensions in quasi 2D system ( $L \times L \times k\sigma$ ) with periodic boundary conditions. While LB captures the three dimensional hydrodynamics associated to the system geometry, squirmers are confined to move on a plane, ensuring that both the component of the velocity perpendicular to the plane and the angular velocity acting off-plane, vanish. For computational convenience, the thickness of the slab is larger than a particle diameter ( $k = 5$ ). We will consider the collective dynamics of semidilute suspensions at  $\phi = 0.10$  (where  $\phi = \frac{\pi}{4}\rho\sigma^2$  and  $\rho = N/L^2$ ) and simulate  $N = 10000$  spheres to minimize finite size effects (corresponding to lateral box sizes of  $L \approx 111r_{cut}$ ). (As a double check, we have also run simulations for larger systems and have not observed significant deviations). A squirmer travels its own size in  $t_0 = \frac{\sigma}{v_s}$ . We have run simulations from 1450 up to 3000  $t_0$ . Once the system reaches steady state, in a time window between 1000 and 2000  $t_0$ , we carry out a systematic analysis of the dynamics of the squirmer suspension, considering  $\xi$  from 1 to  $\infty$  and  $\beta$  from -3 up to 3.

## B. Active Brownian Disks

For the two dimensional Brownian dynamics simulations, each of the  $N$  active disks (with diameter  $\sigma$ ) are

represented by their positions and self-propulsion directions  $\{\mathbf{r}_i, \theta_i\}$ , both satisfying the coupled overdamped Langevin equations,

$$\dot{\mathbf{r}}_i = \frac{D}{k_B T} [\mathbf{F}_{LJ}(\{\mathbf{r}_i\}) + F_p \mathbf{e}_i] + \sqrt{2D} \mathbf{j}_i^T, \quad (5)$$

$$\dot{\theta}_i = \sqrt{2D_r} \eta_i^R, \quad (6)$$

where  $\mathbf{F}_{LJ}$  is the force due to the Lennard-Jones potential (eq. 3),  $F_p$  the magnitude of the self-propulsion which, in the absence of interactions, will move a particle with speed  $v_p = \frac{D}{k_B T} F_p$  and  $\mathbf{e}_i = (\cos \theta_i, \sin \theta_i)$ .  $D$  and  $D_r$  are translational and rotational diffusion constants, which in the low-Reynolds-number regime can be related by  $D_r = 3D/\sigma^2$ . The  $\eta_i^{T,R}$  are Gaussian white noise variables with  $\langle \eta_i(t) \rangle = 0$  and  $\langle \eta_i(t) \eta_j(t') \rangle = \delta_{ij} \delta(t - t')$ . Equations 5 and 6 are tailored for Brownian disks, where the direction of the self-propulsion ( $\theta_i$ ) does not induce a torque (in contrast with the dynamics for Active Brownian Rods [32]).

The Brownian dynamics for disk shaped Active Brownian particles (ABP) we implement evolves in time according to an Euler scheme with a time step of  $5 \cdot 10^{-5} \tau$ , being  $\tau$  the time unit ( $\sigma^2/D$ , where  $D$  is set to  $1 \sigma^2/\tau$ ),  $\sigma$  the length unit and  $k_B T$  the energy unit. The reduced temperature ( $k_B T/\epsilon$ ) is set to 0.2 (being  $1/k_B T = 1$ ). Brownian dynamics simulations are run over  $10^8 \tau$ , and the time a particle travels its own size is  $t_0 = \sigma/v_p$ . We have started measuring only when the system reached a clear steady state.

We have considered the semidilute regime, and analyse the behaviour of a suspension at  $\phi = 0.10$ . To minimize finite size effects, we have simulated  $N = 10000$  self-propelled disks. When setting the propulsion force to zero, we recover the results expected for a dilute suspension of Lennard-Jones passive particles interacting via eq. 3 as in Ref. [50] with the same parameters ( $\phi = 0.1$  and the reduced temperature 0.2). At the chosen temperature and density, the equilibrium counterpart of our system lies in the liquid-vapor coexistence region and forms a steady state distribution of small clusters. When simulating the passive Brownian case ( $F_p = 0$ ), we also recover the results obtained by Matas-Navarro and Fielding[43] for a similar value of  $\phi$  ( $\phi = 0.125$ ) and  $\tilde{D} = 0.2$ : once more, the system forms a steady state cluster distribution.

To quantify the competition between attraction and propulsion, we study the system at different values of  $\xi = \frac{F_p \sigma}{\epsilon}$  (that corresponds to  $P_{agg}^{-1}$  used in Ref.[25, 27]) ranging from 0.5 up to 6, in order to be able to compare with results obtained for squirmers.

## C. Analysis tools

We identify clusters based on a distance criterion: two particles belong to the same cluster whenever their

distance is smaller than  $r_{cl} = 1.8\sigma$  for squirmers and  $r_{cl} = 1.5\sigma$  for ABP (see Appendix).

We evaluate the fraction of clusters of size  $s$ ,  $f(s)$  as a measure of the cluster-size distribution. To calculate  $f(s)$  we apply the same criterion as in Ref. [51]: (i) We arbitrarily subdivide the range of  $s$ -values into intervals  $\Delta s_i = (s_{i,max} - s_{i,min})$ , where we define the total number of clusters within each interval  $\Delta s$  as  $n_i^t$ ; (ii) we assign the value  $n_i = n_i^t / \Delta s_i$  to every  $s$  within  $\Delta s_i$ , and compute the fraction of clusters of size  $s$  as  $f(s) = n_i / N_c$  where  $N_c = \sum_i n_i \Delta s_i$  is the total number of clusters.

We also compute morphological and orientational properties of the clusters, such as their radius of gyration

$$R_g = \sqrt{\sum_{i,j=1}^s \frac{(\mathbf{r}_i - \mathbf{r}_j)^2}{2s}} \quad (7)$$

(dividing by 2 to avoid double counting) and their polar order

$$P = \left| \frac{\sum_{i=1}^s \mathbf{e}_i}{s} \right|. \quad (8)$$

The cluster's orientation with respect to the cluster's translation ( $\mathbf{v}_{CM}$ ) is also determined

$$\Omega(s) = \frac{\mathbf{v}_{CM}(s) \cdot \mathbf{P}(s)}{v_{CM}P} \quad (9)$$

where  $\mathbf{v}_{CM}(s)$  is the cluster center of mass velocity, and  $\mathbf{P}(s)$  is defined as

$$\mathbf{P}(s) = \frac{\sum_{i=1}^s \mathbf{e}_i}{s}. \quad (10)$$

### III. RESULTS

#### A. Mean cluster size

In order to assess when the suspension reaches a steady state [42], we have computed the time dependence of the mean cluster size for the squirmer suspension, as both the mean cluster size and the global polar order must saturate at steady state.

The analysis of the time evolution of these quantities has allowed us to identify three different scenarios. As shown in Fig. 1-a for  $\xi = 0.6$  (strong LJ interactions,  $\xi < 1$ ) squirmer suspensions display coarsening. In this regime attraction dominates over self-propulsion leading to cluster growth. Pushers coarsen faster than pullers due to an intermediate slowdown for the latter. In both cases, the asymptotic coarsening is compatible with an algebraic growth, with exponent  $3/4$ , larger than the previously reported asymptotically coarsening exponent,  $\alpha = 2/3$ , on 2D attractive squirmers at  $\beta = 0$  [43].

Increasing  $\xi$  even further, we find a regime where coarsening depends on the active stress. This regime is shown

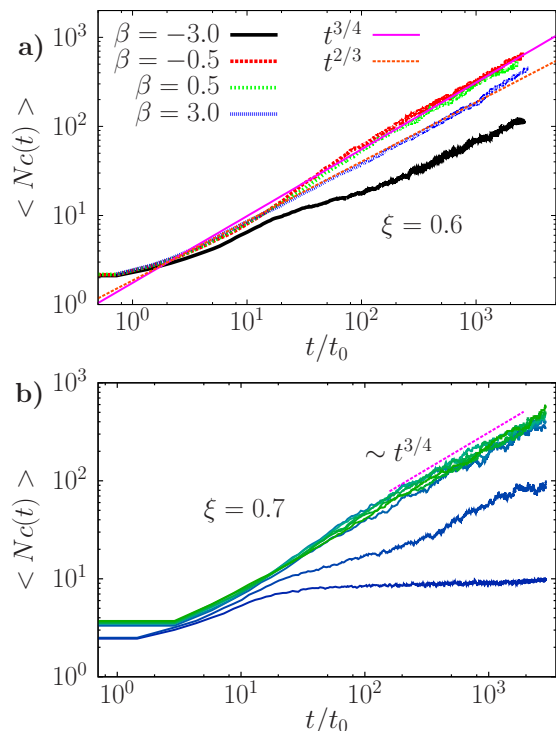


FIG. 1. a) Mean cluster size as a function of time for squirmers with strong LJ interactions: a)  $\xi = 0.6$  and b)  $\xi = 0.7$ . In both panels dashed orange and solid pink curves represent  $\sim t^{2/3}$  and  $t^{3/4}$  respectively and active stress  $\beta$  ranges from  $-3$  to  $3$ .

in Fig. 1-b for  $\xi = 0.7$ . This is a clear example where the collective behaviour of the active suspension depends not only on its degree of activity, but also on the type of hydrodynamic stresses squirmers induce in the surrounding fluid. As we decrease  $\xi$ , the range of  $\beta$  for which coarsening is observed increases asymmetrically between pushers and pullers.

Figure 2 summarizes all results obtained for ABP and squirmers. In both cases, cluster formation is due to the competition between attraction and self-propulsion, as quantified by  $\xi$ .

Figure 2-a displays the mean cluster-size as a function of time for self-propelled spherical Brownian particles in two dimensions at different interaction strength. When attraction is stronger than propulsion ( $\xi = 0.5, 1.0$  and  $1.3$ , dark blue curves), we observe the system coarsening and that the stronger the attraction the faster the coarsening. Whereas when attraction competes with propulsion ( $\xi > 1.3$ ) the system quickly enters a regime of steady state clusters, whose size depends on the propulsion strength (the higher the propulsion, the smaller the clusters).

In Figure 2-b, we observe that the mean cluster size for  $\xi = 1$  is sensitive to the nature of the active hydrodynamics interactions, and changes with  $\beta$ : pushers ( $\beta < 0$ ) reach a steady state faster and the larger the  $|\beta|$  the lower

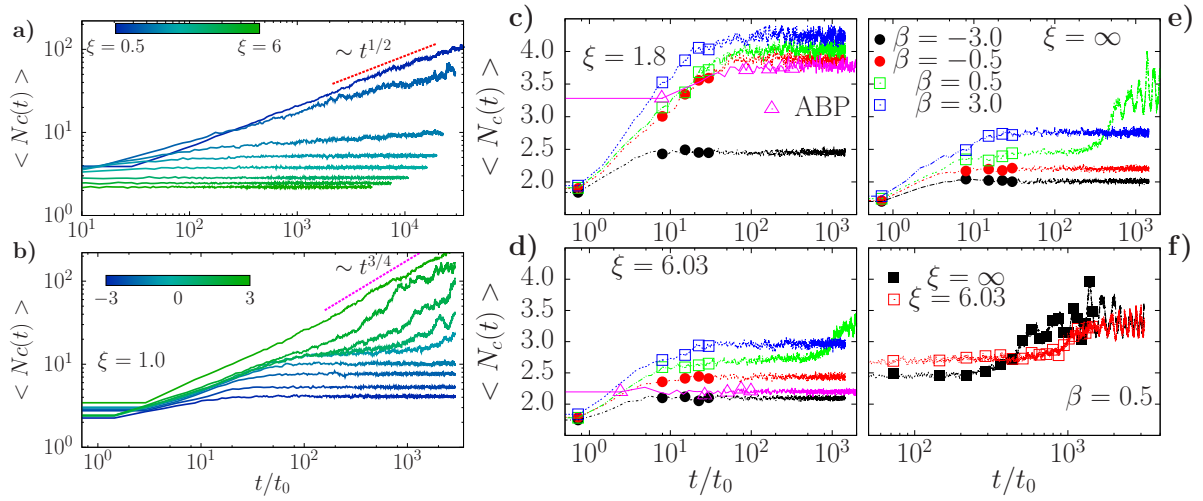


FIG. 2. Mean cluster size as a function of time for different cases. (a) Brownian spherical particles at different values of interaction strength, from  $\xi = 0.5$  to 6. The red line corresponds to the curve  $\sim t^{1/2}$ . (b) Squirmers with  $\xi = 1$  for various values of  $\beta$  from  $-3$  to  $3$ . The pink line correspond to the curve  $\sim t^{3/4}$ . (c) Squirmers with  $\xi = 1.8$ . Circles correspond to  $\beta < 0$  whereas squares to  $\beta > 0$ , pink triangle correspond to ABP with the same interaction strength. (d) Squirmers and ABP with  $\xi = 6.03$ . (e) Squirmers with  $\xi = \infty$  and (f) mean cluster size for  $\beta = 0.5$  with  $\xi = 6.03$  and  $\xi = \infty$  up to  $t/t_0 = 3000$ .

the mean cluster size; whereas pullers,  $\beta \geq 0$ , coarsen. Pullers with  $\beta < 3$  first reach a metastable mean cluster size of about 15 particles at short times, and their mean cluster size grows again due to cluster-cluster interactions: the smaller the  $\beta$  the longer the time a suspension remains in its metastable state.

To ensure the robustness of either the cluster or the coarsening state, we have carried out simulations over longer times and simulations whose initial configuration consisted of all particles forming one big cluster: we observed that while at the beginning the mean cluster size dropped to the metastable state, then grew in the same way as when particles were randomly distributed at the beginning of the simulation.

Cluster formation is caused by attraction competing with self-propulsion. However, for squirmers active stresses modulate this competition. As a result, we observe that pullers promote cluster formation because of their tendency to align to nearby squirmers. Therefore, for a given  $\xi$ , a larger fraction of pullers coarsen compared to pushers of analogous active stress. For an equivalent  $\xi$ , clusters of active Brownian disks are on average larger than squirmers one, indicating that active stresses contribute to break clusters due to an induced hydrodynamic dispersion. However, we cannot exclude that by fine tuning  $\beta$  there may be ranges of  $\xi$  for which the same mean cluster size can be obtained both for ABP and squirmers.

As shown in Figure 2-c-f, when we further increase the activity beyond  $\xi \geq 1.5$  we enter a regime where all suspensions reach a steady state in which squirmers do not merge in one cluster, and the mean cluster size decreases as  $\xi$  increases. When  $\xi = 1.8$  (Figure 2-c) coarsening disappears even for pullers, and a steady state cluster size distribution is reached for all squirmers. ABP with the same  $\xi$  develop a mean cluster size similar to the pushers with a slightly negative value of  $\beta$  ( $\beta = -1/2$ ). Therefore, we conclude that the stress activity dictates the magnitude of the average cluster size, since pullers form larger clusters than pushers.

If we now increase  $\xi$  even further (Figure 2-d), once more we observe all systems reaching a steady state cluster size distribution independently on the value of  $\beta$ . The average cluster size is now smaller than for  $\xi = 1.8$ . For weak pullers ( $\beta = 0.5$ ) the system exhibits a transient arrest: this behaviour could be attributed to the development of metastable clusters, before reaching the stable distribution for longer times. Moreover, these puller suspensions exhibit stronger density fluctuations (as we will discuss later) which could underline this peculiar behaviour. Once more even for higher values of  $\xi$ , ABP with  $\xi = 6.03$  evolve to a mean cluster size similar to weak pushers.

To conclude, we also analyse repulsive squirmers,  $\xi = \infty$  (Figure 2-e and f) where  $\langle N_c(t) \rangle$  behaves in the same way as for  $\xi = 6.03$ . We observe that when  $\beta = 0.5$  and  $\xi$  beyond  $\xi = 6.03$   $\langle N_c(t) \rangle$  oscillates at long times (beyond the meta-stable state), and identify this feature as a third scenario where the mean cluster size of the

suspension has an oscillatory behaviour, associated with a specific parameters range (for  $\xi \gg 1$  and  $0 < \beta < 1$ ). To validate the persistence of the fluctuations, we run these simulations for longer time and conclude that 1) the attraction strength only affects the relaxation time towards this oscillatory regime, 2) the larger the value of  $\xi$  the smaller the relaxation time. Therefore, while the stress generated by the squirmers promotes both alignment and clustering between them, favouring oscillations of the mean cluster size, the attractive interaction partially competes delaying the relaxation to the regime controlled by active stresses.

In Figure 3 we represent instantaneous snapshots for spherical attractive ABP with  $\xi = 1$  (Fig. 3-a) and  $\xi = 4$  (Fig. 3-b) as well as several regimes of squirmers with  $|\beta = 0.5|$  (Figures 3 c to h). For  $\xi = 1$  ABP coarsen, whereas for  $\xi = 4$  a steady state clustering is observed. For squirmers richer behaviour is observed depending on the hydrodynamic character of their active stresses, since for  $\xi = 1$  we observe either coarsening if  $\beta = 0.5$  (Fig. 3-c) or clustering if  $\beta = -0.5$  (Fig. 3-d). Even though coarsening disappears increasing  $\xi$  both for squirmers and for ABP, particles are not distributed in the same way (as shown in Figures 3-b and 3-e and f) and squirmer clusters are smaller, on average, than their Brownian counterparts. Comparing figure 3-g and 3-h, one observe how pullers form clusters of particles moving in the same direction (figure 3-g), that percolate when the collective behaviour only depends on the stress activity. On the contrary, for pushers the suspension is completely homogeneous (Fig. 3-h). In the Supplementary information we have included representative movies to better capture the features reported in Fig. 3.

## B. Density fluctuations in squirmer suspensions

The nature of the emerging clusters and their intrinsic dynamics can be indirectly measured through the number density fluctuations, evaluating the mean number of particles  $\bar{N}$  and the standard deviation  $\Delta N$  as a function of the size of the subsystem in which we partition the suspension. Asymptotically, the standard deviation obeys to a power law,  $\langle \Delta N \rangle \sim N^\alpha$ . If fluctuations are uncorrelated, as in equilibrium,  $\alpha = 1/2$ , whereas suspensions with correlated density fluctuations will be characterized by an exponent  $\alpha > 1/2$ . The system is characterized by giant density fluctuations (GDF) when  $\alpha \geq 1/2$  [52, 53].

Active systems have been shown to display large number density fluctuations, as in bacterial colonies [54] with a scaling exponent  $\alpha = 3/4 \pm 0.03$ , or in computer models of self propelled particles [53, 55] with a maximum value  $\alpha = 0.8$ . These fluctuations in active systems can have different nature: Vicsek-like models, require long-range orientational order [53] whereas the fluctuations of self-propelled rods (SPR) are remarkably different [32] since either polar or apolar long-range or quasi-long-range order are absent. In our case the hydrodynamic signature is

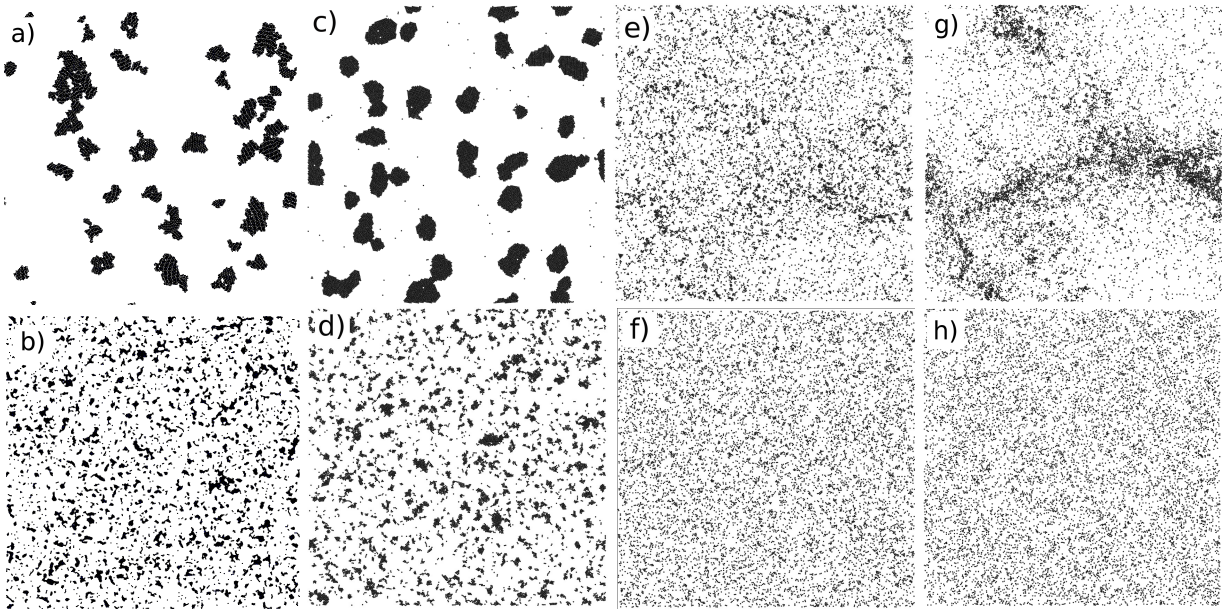


FIG. 3. Snapshots for different values of interaction strength for ABP and squirmers suspensions. The first column represent Active Brownian spheres, whereas all other columns are squirmers. a) ABP with  $\xi = 1$ , b) ABP with  $\xi = 4$ , c) Squirmers with  $\xi = 1$  and  $\beta = 0.5$ , d) Squirmers with  $\xi = 1$  and  $\beta = -0.5$ , e) Squirmers with  $\xi = 5$  and  $\beta = 0.5$ , f) Squirmers with  $\xi = 5$  and  $\beta = -0.5$ , g) Squirmers with  $\xi = \infty$  and  $\beta = 0.5$  and h) Squirmers with  $\xi = \infty$  and  $\beta = -0.5$ . All snapshots for squirmers were taken at  $t/t_0 = 1450$ .

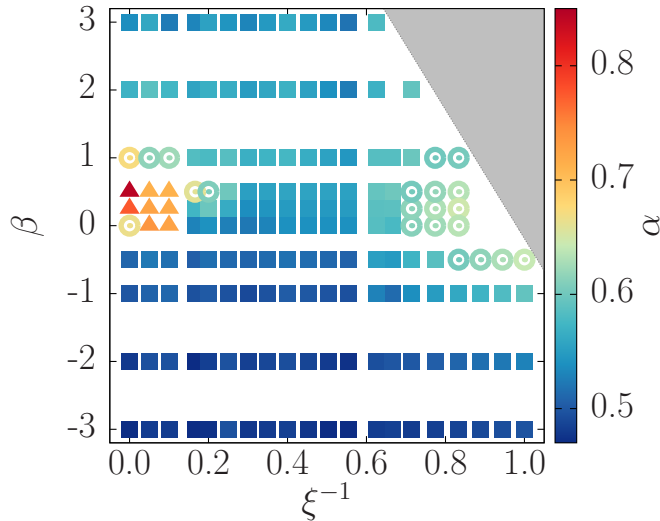


FIG. 4. Colour map of the scaling exponent  $\alpha$  for values of  $\xi$  and  $\beta$  where coarsening is absent. Triangles correspond to  $\alpha > 0.7$ , circles to  $\alpha$  between 0.6 and 0.7, where partially large fluctuations are found, and blue squares are for homogeneous suspensions where  $\alpha < 0.6$ . The gray area represents the values where coarsening is found.

what leads to polar order and the subsequent emergence of fluctuations. [32, 56]

In squirmer suspensions we find that  $\alpha$  depends both

on active stresses and attractive interactions, as shown in Fig. 4 (where the grey area indicates the region of the phase space where coarsening is observed). We estimate exponents between  $(0.47, 0.85)$  and identify three regimes: one with scaling exponent of  $\sim 0.5$  for homogeneous suspensions (blue squares), a second one with intermediate values between 0.6 and 0.7 (green-yellow circles) and a third one when suspensions present large and loosely packed dynamic clusters  $\alpha > 0.7$ , as in the case of squirmers with  $\xi > 5.0$  and  $0 < \beta < 1$  (red-orange triangles).

For the same degree of active stresses, pushers and pullers do not always exhibit the same number density fluctuations: while for pushers  $\alpha$  remains close to  $1/2$  and grows very slowly as the attraction strength increases ( $\xi^{-1} \rightarrow 1$ ), reaching values of  $\alpha = 0.64$  for  $\beta = -0.5$  and  $\xi = 1$ ; pullers with  $\beta > 1$  have an exponent around 0.6, independently of the attraction strength. A value of  $0 \leq \beta \leq 1$  leads to anomalous density fluctuations due to stress activity from a maximum value of  $\alpha$  at  $\xi = \infty$  to a value typical for homogeneous suspensions ( $\alpha \rightarrow 0.5$ ) as  $\xi \rightarrow 1$ .

To conclude, we observe GDF for pullers and for pushers with small  $|\beta|$ , stressing the relevance of hydrodynamic coupling in the morphology of the cluster phase. We observe that  $\alpha > 3/4$ , for weak pullers ( $0 < \beta < 1$ ), correlate with the development of large clusters. Therefore, GDF with large values of  $\alpha$  constitute a signal of collective morphological changes.

### C. Cluster-size distribution

In order to quantify how the interplay between attractive forces and activity determine the dynamic clusters, we have systematically analysed the clusters structures when semidilute active suspensions reach a steady state, by studying the cluster size distribution (CSD) as a function of the activity parameter  $\xi$ , and the active stress generation  $\beta$  (for squirmers).

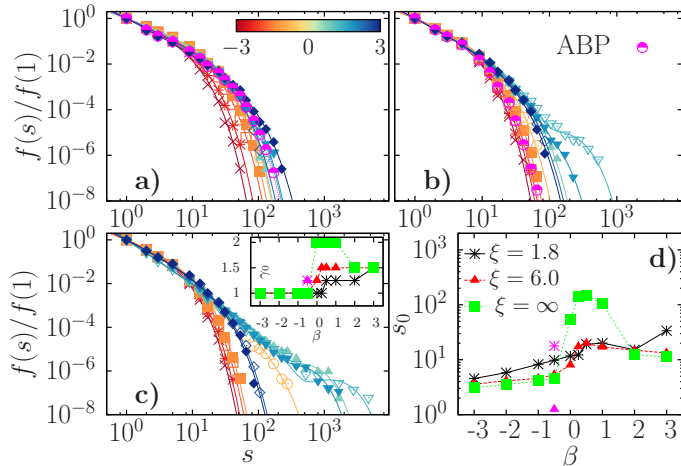


FIG. 5. Cluster-size distribution  $f(s)$  for different values of  $\xi$  and  $\beta$ . Red symbols correspond to pushers  $\beta < 0$  and blue ones to pullers  $\beta > 0$ , yellow for  $\beta = 0$ . Pink points represent the CSD for ABP. Solid lines correspond to fitted curves of eq. (11). a) CSDs with  $\xi = 1.8$ , b) CSDs with  $\xi = 6.03$ , c) CSDs for squirmers with  $\xi = \infty$ , the inset showing the fitted values of the exponent  $\gamma_0$  as a function of  $\beta$  for three different interaction strengths and in pink the fitted parameter for ABP. d) Cluster size cut-off  $s_0$  as a function of  $\beta$  for three different values of  $\xi$ .  $s_0$  obtained by fitting  $f(s)$  to equation (11), in pink the fitted parameter for ABP.

Figure 5 displays the CSD for different values of  $\xi$ , for  $\beta$  in the range between -3 and 3, calculated as the average fraction of clusters  $f(s)$  of a given number of particles  $s$ . Fig. 5-a shows CSD for  $\xi = 1.8$ : the CSD are wider as  $\beta$  increases without reaching a purely algebraic function ( $f(s) \sim s^n$ ). ABP with  $\xi = 1.8$  are characterized by CSD resembling those of weak pushers.

For  $\xi = 6.03$  (Fig. 5-b) CSD for pushers ( $\beta < 0$ ) shows a very weak dependence on the magnitude of the active stress and have approximately the same shape. For pullers CSDs are wider, and pullers with small  $\beta$  develop an inflection point in the distribution for large clusters ( $s \sim 10^2$ ). As  $\beta$  increases to  $\beta > 1$ , the CSDs narrows even further. Whereas ABP display a CSD that resembles those observed for weak pushers, even though for smaller clusters.

In the case of repulsive squirmers (Fig. 5-c,  $\xi = \infty$ ), the CSDs for pushers are narrower and have a very weak dependence on  $\beta$  as in the case of pushers with  $\xi = 6.03$

(red curves in Fig. 5-c); whereas for weak pullers,  $\beta \simeq 1$ , the distributions are wider and characterized by an inflection point more marked at  $s \approx 10^3$  for  $\beta = 0.5$ ; for  $\beta > 1$  the distributions get narrower again but not as much as the corresponding ones for pushers. It is important to notice that, even in the absence of any attraction, generically the CSD width increases only with the active stress (through  $\beta$ ). When  $\beta = 0$  the CSD starts showing an inflection point. For ABP without any attractive interaction we shall expect a very narrow CSD since both density and activity are too small to allow for cluster formation.

From the panels a, b and c of Fig. 5 we deduce that attraction diminishes the probability to generate an inflection point in the CSD for  $0 < \beta < 1$ . This feature indicates that the dynamics of large clusters has fundamentally an hydrodynamic origin.

The CSD can be accurately fitted by

$$\frac{f(s)}{f(1)} = A \frac{\exp(-(s-1)/s_0)}{s^{\gamma_0}} + B \frac{\exp(-(s-1)/z_0)}{s^{-\gamma_0}}, \quad (11)$$

with  $\gamma_0$ ,  $s_0$ ,  $z_0$  and  $B$  constants that depends on  $\beta$  and  $\xi$ , such that  $A = 1 - B$ . The parameter  $s_0$  has been used to control the cutoff at large cluster size [57] and related with the particles density [58, 59]. More recently, the divergence of the cluster size cut-off has been related to the location of the phase separation in a suspension of Brownian self-propelled repulsive disks [55, 57].

Since in Fig. 5-a, for  $\xi = 1.8$  we do not observe an inflection point, we take  $B = 0$  and  $\gamma_0 = 1$  for pushers and pullers with  $\beta < 1/2$ . The value of  $\gamma_0$  will then grow as a function of  $\beta$  (black points in the inset of Fig. 5-c). The CSD for ABP with  $\xi = 1.8$  can be fitted with  $s_0 = 17.9$  and the exponent  $\gamma_0 = 1.25$ : which are values close to the ones for squirmers with  $\beta$  slightly negative.

The CSDs for pushers with  $\xi = 6.03$  corresponds to  $B = 0$  (no inflection), an exponent  $\gamma_0 = 1$ , and  $s_0$  almost independent of  $\beta$ , since the distributions are pretty similar. The CSD for ABP is fitted with  $s_0 = 5.14$  and  $\gamma_0 = 1.25$ , parameters that are similar to the ones fitted for the CSD of pushers with  $\beta$  between  $-1$  and  $-0.5$ .

Once  $\beta$  is non-negative,  $\gamma_0$  grows as a function of  $\beta$  as in the previous case with larger attractions between particles (red circles in the inset of Fig. 5-c), but in this case  $B = 4 \times 10^{-8}$  and  $7 \times 10^{-7}$  for  $\beta = 0.5$  and 1, respectively, due to the presence of an inflection in the distributions (and  $B = 0$  otherwise).

The CSDs for pushers with  $\xi = \infty$  also present  $B = 0$  and  $\gamma_0 = 1$  like pushers with  $\xi = 6.03$ . On the other hand, when  $0 \leq \beta \leq 1$  the CSDs are fitted with  $B \neq 0$  where  $10^{-12} \leq B \leq 10^{-9}$  and  $B = 0$  for  $\beta > 1$ .

To summarize, the CSD curves for pushers never develop an inflection point independently of the interaction strength, thus  $B = 0$ , the power law exponent never change and  $\gamma_0 = 1$  in all cases. The transition to another value of the exponent  $\gamma_0$  depends on the interaction strength, as shown in the inset of Fig. 5, where  $\gamma_0$  changes with  $\beta$  depending on the interaction strength.



Figure 5-d shows how the characteristic cutoff cluster size  $s_0$ , increases with  $\beta$  when the attractive interactions compete with activity ( $\xi = 1.8$ ). The general increase when we move from pushers to pullers always persists, indicating that pullers favours the development of larger cluster sizes. However, when attractive forces become sub-dominant with respect to self propulsion, the region of weak pullers (when self propulsion and active stresses are comparable) is characterized by much wider CSDs which are reflected in a strong increase in the dependence of  $s_0$  on  $\beta$ , with a dominant peak at  $\beta = 1/2$ . Finally, in all the cases where  $B \neq 0$ , we found that  $z_0$  has values similar (the same order of magnitude) to  $s_0$ .

In the case of the CSDs for ABP we found the exponent  $\gamma_0 = 1.25$  for all the studied interaction strengths, whereas  $s_0$  was growing as the attraction increased.

#### D. Radius of gyration

In order to characterize the cluster morphology, we have computed the dependence of the clusters radius of gyration  $Rg(s)$  with their size,  $s$ , from Eq. (7). Fig. 6 displays the mean radius of gyration normalized by the particle radius.

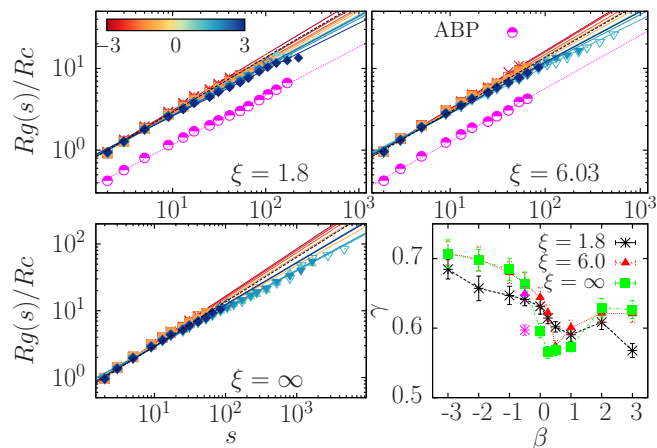


FIG. 6. Radius of gyration  $Rg(s)$  (normalized by the particle's radius) as a function of the cluster-sizes for values of  $\xi$  ranging from 1.8 up to  $\infty$  and  $\beta$  between 3 and  $-3$ . Red symbols correspond to pushers  $\beta < 0$  and blue ones to pullers  $\beta > 0$ . Solid lines represent  $Rg(s) \sim s^\gamma$ . Top-left  $\xi = 1.8$ , and top-right:  $\xi = 6.03$ . Pink data correspond to  $Rg$  for ABP with the same values of  $\xi$ . Bottom-left:  $\xi = \infty$  and Bottom-right:  $\gamma$  exponent as a function of  $\beta$  and  $\xi$ .

We always observe an algebraic dependence,  $Rg \sim s^\gamma$ , with an exponent that depends both on  $\xi$  and  $\beta$ .

When  $\xi = 6.03$  (top-right in fig. 6),  $Rg(s)$  follows an exponent greater than  $2/3$  for pushers, whereas  $Rg(s)$  decreases slower for pullers than for pushers. In fact the exponent  $\gamma$  depends on the  $\beta$  value: the larger the  $\beta$  the larger the exponent, even though always smaller than

$2/3$ . The  $Rg(s)$  slope decreases with  $\beta$  up to  $\beta = 0.5$  where the minimum value for  $\gamma$  is reached, then  $\gamma$  increases as  $\beta$  increases.

Fig. 6 (bottom-right) displays the dependence of the scaling exponent on  $\beta$  for different values of  $\xi$ . For pushers the scaling exponent decreases as  $\beta$  increases. This tendency persists initially for pullers, but changes its trend above  $\beta \simeq 0.5$ , leading to cluster re-expansion, and increases afterwards to saturate around  $\gamma \simeq 0.62$ . Puller clusters are more compact than their pusher counterparts. When activity dominates the cluster morphology becomes indistinguishable from that of repulsive squirmers. In fact, comparing the curves for  $\xi = 1.8$  and  $\xi = \infty$  one can see that active hydrodynamic stresses determine the main changes of the scaling exponent independently of the attractive forces. In particular, the re-expansion observed for pullers increasing active stresses is essentially a hydrodynamic phenomenon. As the attractive forces increase their relative importance, the clusters become more compact but the dependence on  $\beta$  is not significantly altered.

In the case without hydrodynamics, clusters are more compacted as we increase the interaction strength, as expected.  $Rg$  of ABP clusters follow a power law with an exponent of  $\gamma = 0.6$  for  $\xi = 1.8$  which is similar to the exponent for squirmers with slightly negative  $\beta$  at the same interaction strength; if  $\xi = 6.03$  the  $Rg$  for ABP develops an exponent of  $\gamma = 0.65$  which corresponds to the exponent developed by squirmers with a slightly negative  $\beta$  with the same interaction strength.

The values of  $\gamma$  falls between the scaling exponent corresponding to diffusion limited cluster aggregation (DLCA), 0.704, and the reaction limited cluster aggregation (RLCA), 0.62. As we move from pushers to pullers we see that clusters become more compact and get closer to RLCA. The clusters that active suspensions form are always more compact than DLA ones, with  $\gamma = 0.588$ , and definitely more compact than the structure of percolating clusters, with  $\gamma = 0.527$ . Only for  $\beta = 0.5$ , squirmers have an exponent close to the DLA one. This trend is consistent with the increase in density fluctuations and the wider CSD observed for weak pushers.

However, the connection between physical interactions and cluster aggregation mechanisms remains elusive. Even though in colloidal systems the fractal structure of colloidal clusters is thought to be very sensitive to the nature and range of particle attractions [60], we conclude that the crossover from RLCAS to DLCAS-like behavior for squirmers is essentially a hydrodynamic phenomenon.

#### E. Polar order

We analyse the degree of alignment as a function of the cluster size, using Eq. (8). Fig. 7 shows that, generically, the degree of polar order decreases with cluster size.

Pushers (in red) have a faster decay than pullers (in

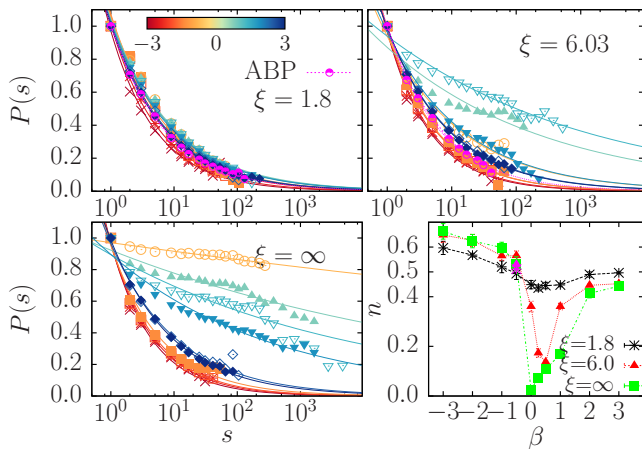


FIG. 7. Polar order parameter  $P$  as a function of the cluster-size for values of  $\xi$  ranging from 1.8 up to  $\infty$  and  $\beta$  between  $-3$  and  $3$ . Red symbols correspond to pushers  $\beta < 0$ , blue ones to pullers  $\beta > 0$ , yellow to  $\beta = 0$ . Solid lines correspond to the fitted curve  $P(s) \sim s^{-n}$  and pink circles to ABP. Bottom-right: Exponent  $n$  as a function of  $\beta$  and  $\xi$ , in pink the fitted parameter for ABP.

blue). In the absence of significant attraction, for  $\xi = \infty$ , we see that for pushers the order decreases algebraically, with a dependence compatible with  $P(s) \sim s^{-1/2}$ , while pullers show a persistent polar order for all cluster sizes. In particular, for  $\beta = 0$  we observe a net polar alignment for all clusters. This strong polar ordering is consistent with the development of a global polar phase that displays its maximum orientation in  $\beta = 0$  [42].

As the attraction plays a more relevant role, the degree of polarity for pullers decays and eventually the degree of ordering in the clusters is independent of  $\beta$ . Therefore, the decay  $P(s) \sim s^{-1/2}$  is essentially due to the competition between self propulsion and attraction even though near field hydrodynamic coupling plays a relevant role because in all cases, even at small  $\xi$ , ABP clusters show a larger degree of polar ordering than pusher squirmers. For ABP, at  $\xi = 6.03$  and  $\xi = 1.8$ ,  $P(s)$  has a slower decay as  $s^{-1/2}$ . This means that particles within a cluster maintain their polar order better than pushers do, due to the fact that the rotation induced by hydrodynamics helps to destroy polar ordering [43].

When  $\xi = 6.03$  (top-right panel) pushers show a decay with an exponent  $n > 0.5$ , whereas pullers with  $\beta < 1$  drastically change their behaviour compared to pullers at  $\xi = 1.8$  showing big clusters with high polar order. Clusters of ABP on the contrary, do not suffer any change in their polarity and  $P(s) \sim s^{-1/2}$  independently of the interaction strength.

In order to clarify whether clusters move in the same direction as the particles that constitute them, we have computed for the squirmers case the cluster orientation with respect to the cluster's center-of-mass velocity,  $\Omega$ , as a function of the cluster size, according to Eq. (9), as

shown in Fig. 8.

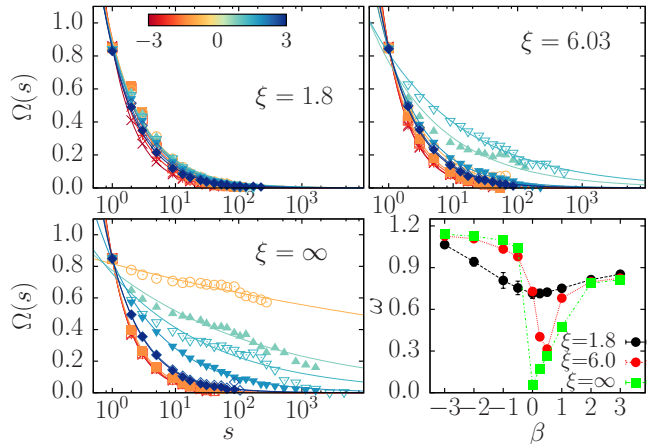


FIG. 8.  $\Omega$  as a function of the cluster-size for values of  $\xi$  ranging from 1.8 up to  $\infty$  and  $\beta$  between  $-3$  and  $3$ . Solid lines correspond to  $\Omega(s) \sim s^{-\omega}$ . Top-left:  $\xi = 1.8$ , Top-right:  $\xi = 6.03$ , Bottom-left:  $\xi = \infty$ . Bottom-right:  $\omega$  exponent value fitted as a function of  $\beta$  and  $\xi$ .  $\Omega(s)$  is normalized by the overdamped velocity reached by one squirmer ( $v_s = 2/3B_1$ ).

In all cases we observe a decay of  $\Omega$  with cluster size, indicating that the direction of motion of the cluster is progressively decorrelated from the average cluster alignment. The slower decay in  $\Omega$  at large  $\xi$  for pullers, when hydrodynamic stresses dominate, indicates that there is a strong correlation between the degree of polarity and the direction of motion of the cluster.

When attraction is reduced (top-right panel Fig. 8) pullers with  $\beta < 1$  have a slow decay given that it is possible to find a partial orientation for big clusters (as shown in figure 7). When  $\beta = 0$  without attractions the clusters orientation decay is very slow (yellow circles in the bottom-left panel of Fig. 8), almost independent of cluster size, given that in this case the global aligned state is stable. Therefore, we have fitted  $\Omega(s)$  to a power law  $s^{-\omega}$ , and the corresponding curves are displayed in Fig. 8 (bottom-right panel), showing a reasonable agreement. The bottom right panel of Fig. 8) shows the dependence of  $\omega$  both on  $\beta$  and  $\xi$ . In general, the decay of  $\Omega$  is slower for pullers than for pushers, due to the larger degree of polar order of the former. As  $\xi$  decreases, the attractive interactions become more dominant and the dependence on active stresses weakens. However, even for the smallest  $\xi$  we still see that pushers have a weaker degree of correlation.

#### IV. DISCUSSION AND CONCLUSIONS

In this paper we have carried out a systematic study of semi-dilute suspensions of interactive squirmers restricted to swim in a plane surrounded by an unconfined fluid. We have seen that active hydrodynamic stresses

give rise to a steady state characterized by dynamic clusters. The properties and character of these clusters are sensitive to the competition between self-propulsion, induced hydrodynamic flows through active stresses and direct short-ranged attractive Lennard-Jones particle isotropic interactions. We have identified the relevant dimensionless parameters that determine the competition between self-propelling and attractive forces,  $\xi$ , which can be regarded as an effective Péclet number, and the relative relevance between self-propulsion and active stresses,  $\beta$ .

The systematic study of the system as a function of ( $\xi$ ,  $\beta$ ), has allowed us to identify three regimes associated to the intrinsic motion of such suspensions. When squirmers attractions dominate over self-propulsion, squirmers aggregate and display coarsening. When attractive forces competes with self-propulsion a steady state is reached, where squirmers are characterized by a cluster size distribution. The transition between these two regimes is a function both of  $\xi$ , and the character of the induced active stresses,  $\beta$ . This fact already shows that the collective behaviour of an active suspension is not only a function of its degree of activity, quantified by  $\xi$ , but rather on the details of the hydrodynamic coupling. When activity dominates we have seen that in some situations the steady state sustains an oscillatory behaviour. In this third regime we have analysed the collective behavior over time scales large compared to these intrinsic oscillations.

We have focused on the regimes where dynamic clusters are stable, typically  $\xi > 1$ , and have quantified the cluster size distributions to classify the emerging steady states. Generically, all the CSDs can be fitted to a bimodal cutoff algebraic shape. The shape of this CSDs is basically prescribed by hydrodynamic interactions. The Lennard-Jones attraction modulates the cutoff distance and leads typically to larger clusters for a given value of  $\beta$ , except in the regime of weak pullers, where attraction disrupts significantly the bimodal shape of the CSD and the strong density fluctuations that characterize this regime. In this case attraction increases significantly the cutoff distance for the CSDs. These fluctuations in the mean size aggregate and the bimodal shape of the CSD emerge purely because of hydrodynamic interactions, since they appear only for weak pullers and very low attraction. Moreover, the active stress given by  $\beta$  re-orientes and polarizes the particles in the dynamic clusters (see Figs. 7 and 8 and movies in the Supplementary Information). A similar coordinated behaviour has been observed with SPR without hydrodynamic interactions [32], where aggregates with intrinsic topological defects grow. Such defects originate highly compressed structures, whose active stresses lead to the fluctuations in the aggregate boundary and the ejection of polar clusters. Thus, the analogy between both systems suggests that aggregate fluctuations might be not model-dependent. One could try to map the active stress induced by  $\beta$  in squirmer aggregates with the active stress induced by topological de-

fects in SPR. Alternatively, one could tune the squirmer aspect ratio [61] since it is known that elongated squirmer suspensions develop a variety of collective motion, including ordering, aggregation and whirls; such morphologies depend on the hydrodynamic signature, given by  $\beta$ , and the particle shape.

In this work we have considered the general case of disks and spheres to spotlight purely the effect of the hydrodynamic interactions. We believe that particle shape plays an important role in the formation of emerging collective patterns [61], and it deserves a study on its own.

We have further compared the properties of the cluster phase of squirmers with the one generated by Active Brownian Disks. In the latter case there are no stresses due to the surrounding fluid, and the only relevant parameter is  $\xi$ , the effective Péclet number. We have found that when attraction competes with activity, ABP form larger clusters than squirmers at equivalent  $\xi$  and the properties of the cluster phase resemble those of weak pushers. However, when activity dominates the CSDs are similar to the CSDs of pushers with the same interaction strength.

The radius of gyration of the observed clusters also identifies the impact of active stresses. We have found that the exponent of the dependence of the radius of gyration on cluster size corresponds to clusters that are always more compact than DLA and move from DLCA to RLCA as active stresses change from pushers to pullers. Attractive forces lead to more compact clusters, but do not change qualitatively the trend promoted by active stresses. When attractive interactions compete with activity we find that clusters shrink as  $\beta$  grows, while when activity dominates a contraction-expansion effect occurs for pullers. Squirmers form generically polarized clusters, but the degree of ordering decreases with cluster size, showing again a strong difference between pullers and pushers. The polar order of the clusters is reduced when hydrodynamic interactions are present in the case where attraction competes with the activity, thus ABP clusters are more aligned. This characteristic effect however is not observed once the activity dominates the attractive interactions.

Therefore, we have shown that hydrodynamics alone can sustain a cluster phase of active swimmers (pullers), while ABP form cluster phases due to the competition between activity and self-propulsion. The structural properties of the cluster phases of squirmers and ABP are similar, although squirmers show sensitivity to active stresses. ABP resemble weakly pushers squirmer suspensions in terms of CSDs, structure of the radius of gyration on cluster size and degree of cluster polarity.

## ACKNOWLEDGEMENTS

FA acknowledges CONACYT-CECTI (México) through Grant No. 214151 for financial support. FA and IP thank MINECO (Spain) through FIS2015-67837-P,

DURSI Project 2014SGR-922. IP also acknowledges the support of Generalitat de Catalunya under program Icrea Academia for financial support. CV acknowledges the EU project 322326-COSAAC-FP7-PEOPLE-CIG-2012, the National Project FIS2013-43209-P and a Ramon y Cajal tenure track. We thank the KITP at the University of California, Santa Barbara, where they

were supported through National Science Foundation Grant NSF PHY11-25925. This work was possible thanks to the access to MareNostrum Supercomputer at Barcelona Supercomputing Center (BSC) and also through the Partnership for Advanced Computing in Europe (PRACE). This article is based upon work from COST Action MP1305, supported by COST (European Cooperation in Science and Technology)

- 
- [1] F. Schweitzer, *Brownian Agents and Active Particles: Collective Dynamics in the Natural and Social Sciences*, Springer, Berlin, (2003).
- [2] E. Lauga and T.R. Powers, Rep. Prog. Phys. **72**, 096601 (2009).
- [3] I.S. Aranson, Comptes Rendus Physique **14**, 518 (2013).
- [4] C. Bechinger, R. Di Leonardo, H. Löwen, C. Reichhardt, G. Volpe and G. Volpe arXiv:1602.00081 (2016).
- [5] T. Vicsek and A. Zafeiris, Phys. Rep. **517**, 71 (2012).
- [6] I. Theurkauff, C. Cottin-Bizonne, J. Palacci, C. Ybert, and L. Bocquet, Phys. Rev. Lett. **108**, 268303 (2012).
- [7] S. Thutupalli, R. Seemann and S. Herminghaus, New J. Phys. **13**, 073021 (2011).
- [8] A. Rabani, G. Ariel, A. Be'er, PLoS ONE **8**, 12 (2013).
- [9] A.P. Petroff, X-L. Wu and A. Libchaber Phys. Rev. Lett. **114**, 158102 (2015).
- [10] S. A. Mallory, A. Šarić, C. Valeriani, and A. Cacciuto Phys. Rev. E **89**, 052303 (2014)
- [11] S. C. Takatori, W. Yan, and J. F. Brady, Phys. Rev. Lett. **113**, 028103 (2014).
- [12] S. C. Takatori and J. F. Brady, Phys. Rev. E **91**, 032117 (2015).
- [13] A. P. Solon, J. Stenhammar, R. Wittkowski, M. Kardar, Y. Kafri, M. E. Cates, and J. Tailleur, Phys. Rev. Lett. **114**, 198301 (2015).
- [14] R. G. Winkler, A. Wysocki, and G. Gompper, Soft Matter **11**, 6680 (2015).
- [15] A. P. Solon, Y. Fily, A. Baskaran, M. E. Cates, Y. Kafri, M. Kardar, and J. Tailleur, Nat. Phys. **11**, 673 (2015).
- [16] Y. Fily and M. C. Marchetti, Phys. Rev. Lett. **108**, 235702 (2012).
- [17] J. Tailleur and M.E. Cates Phys. Rev. Lett. **100**, 218103 (2008).
- [18] G. S. Redner, M. F. Hagan, and A. Baskaran, Phys. Rev. Lett. **110**, 055701 (2013).
- [19] A. Wysocki, R. G. Winkler, and G. Gompper, Europhys. Lett. **105**, 48004 (2014).
- [20] M. E. Cates, and J. Tailleur, Ann. Rev. Cond. Matt. Phys. **6**, 219 (2015).
- [21] J. Stenhammer, A. Tiribocchi, R. Allen, D. Marenduzzo, and M. E. Cates, Phys. Rev. Lett. **111**, 145702 (2013).
- [22] T. Speck, J. Bialké, A.M. Menzel, and H. Löwen, Phys. Rev. Lett. **112**, 218304 (2014).
- [23] A. Zöttl, and H. Stark, Phys. Rev. Lett. **112**, 118101, (2014).
- [24] P. Ball, Physics **6** 134 (2013).
- [25] V. Prymidis, H. Sielcken and L. Filion, Soft Matter, **11**, 4158 (2015).
- [26] G.S. Redner, A. Baskaran, and M. F. Hagan, Phys. Rev. E **88**, 012305 (2013).
- [27] M. Mognetti, A. Šarić, S. Angioletti-Uberti, A. Cacciuto, C. Valeriani, and D. Frenkel, Phys. Rev. Lett. **111**, 245702 (2013).
- [28] Clarion Tung, Joseph Harder, C. Valeriani and A. Cacciuto Soft Matter, **12**, 555 (2016).
- [29] R. Matas-Navarro, R. Golestanian, T.B. Liverpool, and S.M. Fielding, Phys. Rev. E **90**, 032304 (2014).
- [30] T. Ishikawa and T. J. Pedley, Phys. Rev. Lett. **100**, 088103 (2008).
- [31] I. Llopis, and I. Pagonabarraga, Europhys. Lett. **75**, 999 (2006).
- [32] S. Weitz, A. Deutsch, and F. Peruani, Phys. Rev. E **92**, 012322 (2015).
- [33] J. Schwarz-Linek, C. Valeriani, A. Cacciuto, M. Cates, D. Maren-duzzo, A. Morozov and W. Poon, Proc. Natl. Acad. Sci., **109**, 4052 (2012).
- [34] A. Suma, G. Gonnella, D. Marenduzzo and E. Orlandini Europhys. Lett. **108**, 56004 (2014).
- [35] J. Palacci, S. Sacanna, A. P. Steinberg, D. J. Pine, and P. M. Chaikin, Science **339**, 936 (2013).
- [36] G. S. Redner, A. Baskaran and M. F. Hagan, Phys. Rev. E, **88**, 012305 (2013).
- [37] M.C. Marchetti, J.F. Joanny, S. Ramaswamy, T.B. Liverpool, J. Prost, M. Rao and R. Aditi Simha, Rev. Mod. Phys. **85**, 1143 (2013).
- [38] M. J. Lighthill. *Communications on Pure and Applied Mathematics*, **5**(2), 109, (1952).
- [39] S. Ramachandran, P.B.S. Kumar and I. Pagonabarraga, EPJE **20**, 151 (2006).
- [40] I. Llopis and I. Pagonabarraga, J. Non-Newtonian Fluid Mech. **165**, 946 (2010).
- [41] I. Pagonabarraga and I. Llopis, Soft Matter **9**, 7174 (2013).
- [42] F. Alarcón and I. Pagonabarraga, *J. Mol. Liq.*, **185**, 56 (2013).
- [43] R. Matas-Navarro and S.M. Fielding, Soft Matter, **11**, 7525 (2015).
- [44] T. Ishikawa, M.P. Simmonds, T.J. Pedley, *J. Fluid Mech.* **568**, 119 (2006).
- [45] T. Ishikawa and T.J. Pedley, *J. Fluid Mech.* **588**, 437 (2007).
- [46] M.E. Cates, J.C. Desplat, P. Stansell, A.J. Wagner, K. Stratford, R. Adhikari, I.Pagonabarraga, , Phil. Trans. Roy. Soc. A **363**, 1917 (2005).
- [47] S. Succi, *The Lattice Boltzmann Equation: For Fluid Dynamics and Beyond* (Oxford University Press, Oxford, 2001).
- [48] N.-Q. Nguyen and A. J. C. Ladd, *Phys.Rev.E*, **66**, 046708 (2002).
- [49] K. Stratford and I. Pagonabarraga, *Comput. Math. Appl.*, **55**, 1585 (2008).

- [50] B.Smit, J. Chem. Phys. **96** 8639 (1992).
- [51] C. Valeriani, E. Sanz, P.N. Pusey, W.C.K. Poon, M.E. Cates and E. Zaccarelli, *Soft Matter* **8**, 4960 (2012).
- [52] V. Narayan, S. Ramaswamy, N. Menon, *Science*, **317** 105108 (2007).
- [53] H. Chate, G. Ginelli, G. Gregoire, G. Raynaud, *Phys Rev E*, **77**, 046113 (2008).
- [54] H.P. Zhang, A. Be'er, E.L. Florin, H.L. Swinney, Proc. Natl. Acad. Sci., **107** (31) 13626 (2010).
- [55] Y. Fily, S. Henkes and M. C. Marchetti, *Soft Matter* **10**, 2132 (2014).
- [56] S. Dey et al., Phys. Rev. Lett. **108**, 238001 (2012).
- [57] D. Levis and L. Berthier, *Phys. Rev. E* **89**, 062301 (2014).
- [58] F. Peruani, A. Deutsch, and M. Bär, *Phys. Rev. E* **74**, 030904 (2006).
- [59] F. Peruani and M. Bär, *New Journal of Physics* **15**,065009 (2013).
- [60] J. Stankiewicz, M.A. Cabrerizo Vílchez and R. Hidalgo Alvarez, Phys. Rev. E **47**, 2663 (1993).
- [61] K. Kyoya, D. Matsunaga, Y. Imai, T. Omori and T. Ishikawa, Phys. Rev. E **92**, 063027 (2015).
- [62] J. R. Blake, *Journal of Fluid Mechanics*, **46**(01), 199, (1971).
- [63] I. Pagonabarraga, I. Llopis, *Soft Matter* **9**, 7174 (2013).

## V. APPENDIX

### A. Squirmer model

We have used the well known model for microswimmers developed by Lighthill [38] and improved by Blake [62] (proposed to model the locomotion of ciliated microorganisms) in order to simulate self-propelled particles with hydrodynamics interactions. This mode, named squirmer, considers a spherical particle with an internal activity that induces an effective axisymmetric velocity on its surface. Accordingly, the velocity field is defined in terms of two components that depend on the two polar coordinates  $(r, \theta)$ . Therefore, this velocity can be written as two independent terms, a radial  $u_r$  and a polar  $u_\theta$  term

$$\begin{aligned} u_r|_{r=R_p} &= \sum_{n=0}^{\infty} A_n(t) P_n\left(\frac{\mathbf{e}_1 \cdot \mathbf{r}}{R_p}\right), \\ u_\theta|_{r=R_p} &= \sum_{n=0}^{\infty} B_n(t) V_n\left(\frac{\mathbf{e}_1 \cdot \mathbf{r}}{R_p}\right), \end{aligned} \quad (12)$$

where  $\mathbf{r}$  represents the position vector with respect to the squirmer's center (always pointing to the particle surface so that  $|\mathbf{r}| = R_p$ );  $\mathbf{e}_1$  prescribes the intrinsic self-propelling direction, (which moves rigidly with the particle and determines the direction along which a single squirmer displaces);  $P_n$  stands for the  $n$ -th order Legendre polynomial and  $V_n$  is defined as

$$V_n(\cos \theta) = \frac{2}{n(n+1)} \sin \theta P'_n(\cos \theta). \quad (13)$$

The amplitudes  $A_n(t)$  and  $B_n(t)$  are periodic functions determining the flow induced by the beating cilia on the squirmer's surface and  $\theta$  is the angular polar coordinate. Since the cilia wave stroke is faster than the squirmer displacement, we can replace the time dependent amplitudes at the boundary, eqn. (12), by their effective averaged amplitudes over a stroke period,  $B_n(t) = B_n$ . Moreover, we neglect the radial changes of the squirmering motion,  $A_n(t) = 0$ .

At low Reynolds numbers, the flow induced by a squirmer can be obtained by solving the Stokes and continuity equations

$$\begin{aligned} \nabla p &= \nu \nabla^2 \mathbf{u}, \\ \nabla \cdot \mathbf{u} &= 0. \end{aligned} \quad (14)$$

for the fluid pressure,  $p$ , and velocity fields,  $\mathbf{u}$ , subject to the boundary conditions, Eq. 12 [44, 63]. The mean fluid

flow induced by squirmer can be expressed as

$$\begin{aligned} \mathbf{u}(\mathbf{r}) &= B_1 \mathbf{e}_1 \left( -\frac{1}{3} \mathbf{I} + \frac{\mathbf{r}\mathbf{r}}{r^2} \right) \left( \frac{R_p}{r} \right)^3 \\ &+ \sum_{n=2}^{\infty} B_n \left( \frac{R_p^{(n+2)}}{r^{(n+2)}} - \frac{R_p^n}{r^n} \right) P_n \left( \frac{\mathbf{e}_1 \cdot \mathbf{r}}{r} \right) \frac{\mathbf{r}}{r} \\ &+ \sum_{n=2}^{\infty} B_n \mathbf{e}_1 \left( 1 - \frac{\mathbf{r}\mathbf{r}}{r^2} \right) \\ &\times \left( \frac{n R_p^{(n+2)}}{2r^{(n+2)}} - \frac{(n-2) R_p^n}{2r^n} \right) \frac{V_n \left( \frac{\mathbf{e}_1 \cdot \mathbf{r}}{r} \right)}{\sqrt{1 - \frac{\mathbf{e}_1 \cdot \mathbf{r}}{r}}}. \end{aligned} \quad (15)$$

A squirmer particle swims force and torque free at a constant speed of magnitude  $v_s = \frac{2}{3} B_1$  along  $\mathbf{e}_1$  with respect to the solvent.

We consider a simplified version of the squirmer model, and take  $B_n = 0$  when  $n > 2$ , keeping only the first two terms in the general expression of Eq. (15). The two non-vanishing terms are enough to model two essential features of the impact that squirmers have on the surrounding medium: while the polarity is related to the squirmer self-propulsion through the coefficient  $B_1$ , the active stresses are induced by the apolar term  $B_2$ . The squirmer's active stress can be quantified in terms of the squirmer self-propulsion by  $\beta = B_2/B_1$  [44]: if  $\beta > 0$  the squirmer behaves as puller whereas if  $\beta < 0$  it behaves as a pusher. Therefore, the average fluid flow generated in this simplified model by a squirmer can be written as

$$\begin{aligned} \mathbf{u}(\mathbf{r}) &= -\frac{1}{3} \frac{R_p^3}{r^3} B_1 \mathbf{e}_1 + B_1 \frac{R_p^3}{r^3} \mathbf{e}_1 \cdot \frac{\mathbf{r}\mathbf{r}}{r^2} \\ &- \frac{R_p^2}{r^2} B_2 P_2 \left( \frac{\mathbf{e}_1 \cdot \mathbf{r}}{r} \right) \frac{\mathbf{r}}{r}. \end{aligned} \quad (16)$$

The first two terms of equation (16) represent a dipolar field, similar to the one generated by an electric dipole. The direction and strength of the fluid flow is specified by the polarity term  $B_1 \mathbf{e}_1$  in analogy with the electric moments. In turn, the  $B_2$  term models a quadrupolar field.  $B_2$  is equivalent to the strength of a quadrupole for a symmetric arrangement of electric dipoles, when the dipole moments vanish. Then, taking into account that we have only two non-zero terms, the boundary conditions on the surface of the squirmers depicted in equations (12) can be written as

$$\begin{aligned} u_r|_{r=R_p} &= 0, \\ u_\theta|_{r=R_p} &= B_1 V_1(\cos \theta) + B_2 V_2(\cos \theta). \end{aligned} \quad (17)$$

Where  $u_r$  and  $u_\theta$  are the radial and tangential components of the fluid velocity  $\mathbf{u}$ .

### B. Identifying clusters in the suspension.

To start with, we compute the radial distribution function of the Lennard-Jones fluid at the  $\phi$  studied in the

manuscript (only considering configurations in the time interval when the system is in steady state). From Figure 9 we already observe that the system with pullers is more ordered than the system with pushers. In order to detect the clusters in the suspension, we use the first minimum ( $r_{cl}$ ) of the radial distribution function and identify particles within this distance as neighbours belonging to the same cluster.

Even though the  $g(r)$  depends on the hydrodynamic feature and the interaction strength, in Figure 9 we show that a value of  $r_{cl} = 1.8\sigma$  is compatible with all chosen values of  $\xi$  and  $\beta$ . Whereas the  $g(r)$ s for ABP have their first minimum at  $r_{cl} = 1.5\sigma$ , this difference between squirmers and ABP come from the fact that squirmers needs a soft repulsive potential for short distance ( $\sim 1.1\sigma$ ) in order to avoid overlapping among them.

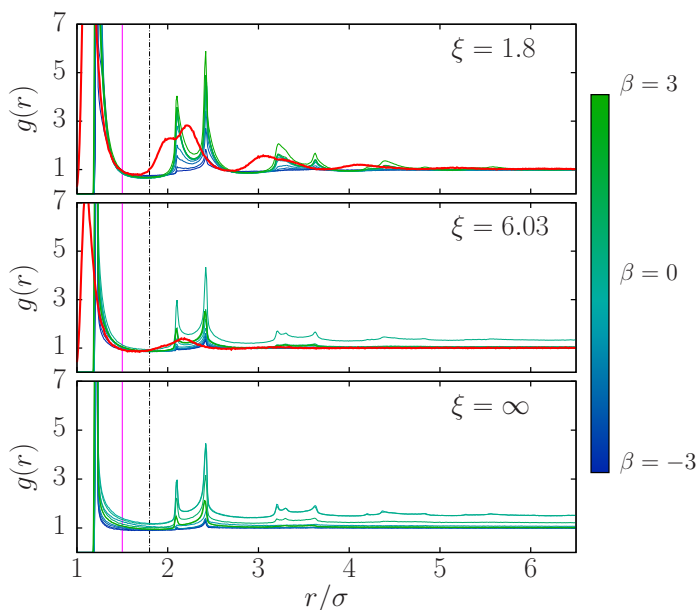


FIG. 9. Radial distribution functions  $g(r)$  for three different values of  $\xi = \{1.8, 6.03, \infty\}$ . The color code of the curves is as a function of  $\beta$ . The  $g(r)$ s for ABP are plotted in red. Black line represents the chosen value of  $r = r_{cl}$  for squirmers, while pink line is  $r_{cl}$  for ABP.

One important remark about the radial distribution function around  $r_{cl}$  is that it is quite flat, being the first and second coordination shell not too close to each other. Therefore, choosing any value within this minimum is not going to affect the cluster size.

In Figure 10, we show the cluster-size distribution functions for different values of  $\beta$  at  $\xi = 1.8$ , using three different values of  $r_{cl} = \{1.3, 1.5, 1.8\}\sigma$ . As expected, the CSDs follow the same power law with an exponential tail behaviour for the three values of  $r_{cl}$ , even though they move to larger clusters for larger values of  $r_{cl}$  for pushers (that are less ordered, as shown in Figure 9).

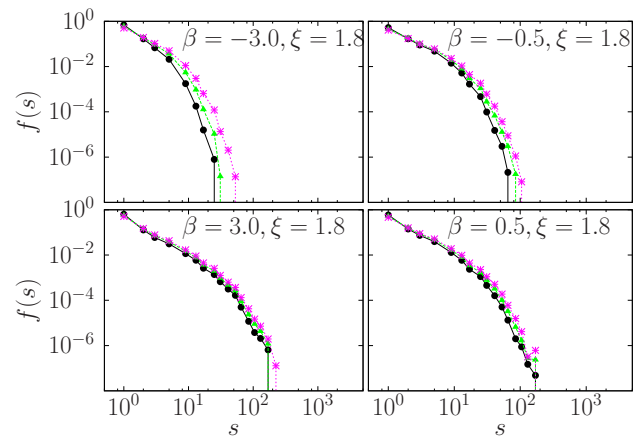


FIG. 10. Cluster-size distribution  $f(s)$  for values of  $\xi = 1.8$ . Black circles correspond to  $r_{cl} = 1.3\sigma$ , green triangles to  $r_{cl} = 1.5\sigma$ , magenta stars to  $r_{cl} = 1.8\sigma$ . The chosen values for  $\beta$  and  $\xi$  are indicated in the legend.

### C. Values of $\Delta s_i$ used to compute $f(s)$

When computing the cluster-size distribution, we group clusters of an average size  $s_i$  in bins with width  $\Delta s_i = (s_{i,max} - s_{i,min})$  as in Ref. [51] (Table I).

TABLE I. Cluster-size intervals  $\Delta s_i = [s_{i,max}, s_{i,min}]$ , centred around  $s_i$ .

$[s_{i,max}, s_{i,min}]$	$s$	$[s_{i,max}, s_{i,min}]$	$s$	$[s_{i,max}, s_{i,min}]$	$s$
1	1	[36,45]	41	[451,600]	526
2	2	[46,55]	51	[601,1000]	801
3	3	[76,95]	81	[1001,1300]	1151
[4,7]	5	[96,120]	109	[1301,2000]	1651
[8,11]	9	[121,140]	131	[2001,3500]	2751
[12,15]	14	[141,200]	171	[3501,5000]	4251
[16,21]	17	[201,250]	226	[5001,7000]	6001
[22,27]	25	[251,300]	276	[7001,10000]	8501
[28,35]	32	[301,450]	376		

### D. Finite-size effects

In Figure 11 we represent the cluster-size distribution for different values of  $\xi$  and  $\beta$  evaluated at the same  $\phi = 0.1$  for two different system sizes,  $N = 10^3$  with filled symbols and  $N = 10^4$  with empty symbols.

Finite-size effects are not present neither when  $\xi = 1.8$  nor when  $\xi = 6.03$ : in both cases,  $f(s)$  obtained for the small system size coincides with the one obtained for the larger system. However, when  $\xi = \infty$  the results obtained for the small and large system only coincide for small clusters and deviate for larger ones. This is due to

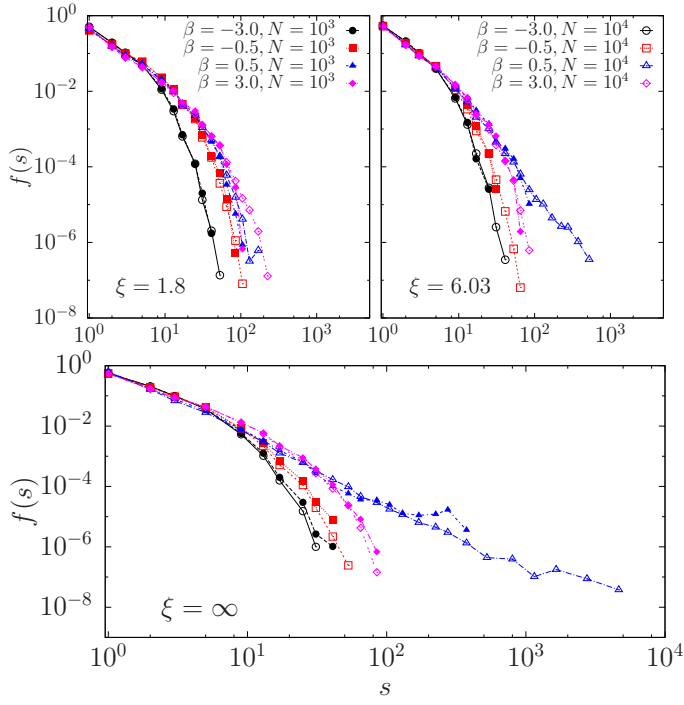


FIG. 11. Cluster-size distribution  $f(s)$  for values of  $\xi = \{1.8, 6.03, \infty\}$ . In all panels, solid symbols are for small systems with  $N = 10^3$  whereas solid symbols are for big systems with  $N = 10^4$ .

the fact that at  $\xi = \infty$  cluster formation is originated by hydrodynamics (long range) interactions, thus affected by the system size.

We now evaluate the clusters' radius of gyration for two different system sizes. In Figure 12 we represent the radius of gyration normalized by the particle's radius for different values of  $\xi$  and  $\beta$ . The symbols are the same as in Figure 11.

As shown in the figure, there are not finite-size effects in the radius of gyration of the clusters despite the chosen value of  $\xi$ .



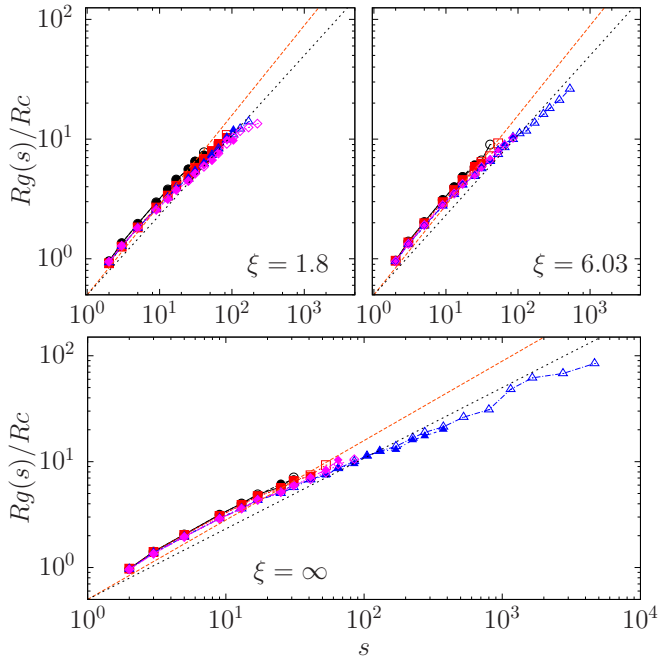


FIG. 12. Radius of gyration  $R_g(s)$  (normalized by the particle's radius  $R_c$ ) as a function of the cluster-size for values of  $\xi = \{1.8, 6.03, \infty\}$ . The symbols are the same as in Figure 11. Orange dashed curve and pointed black curve are a guide to the eye and represent  $s^{3/4}$  and  $s^{2/3}$  respectively.